Journal of Applied Fluid Mechanics, Vol. 17, No. 1, pp. 205-218, 2024.
Available online at www.jafmonline.net, ISSN 1735-3572, EISSN 1735-3645.
https://doi.org/10.47176/jafm.17.1.1985

Novel CFD and DMST Dual Method Parametric Study and Optimization of A Darrieus Vertical Axis Wind Turbine

M. Akhlaghi†, M. Asadbeigi and F. Ghafoorian

Turbomachinery Research Laboratory, Department of Energy Conversion, School of Mechanical Engineering, Iran University of Science and Technology, Tehran, Iran

†*Corresponding Author Email: Mohammad.akhlaghi@iust.ac.ir*

ABSTRACT

The deteriorating effects of greenhouse gases resulting from the use of fossil fuels have led to increased public attention to renewable energy sources, with wind energy being a particularly favored option. This prompted the development of various wind turbine types' efficiency. This study intends to explore the influence of key design parameters consisting of the number of blades, blade chord length, helical angle, and J-shaped blade on the performance and self-starting ability of a Darrieus VAWT. Furthermore, implementing an efficient optimization model to obtain maximum power based on the numerical findings. To achieve this, two different numerical modeling approaches, namely Computational Fluid Dynamics (CFD) and Double Multi-Streamtube (DMST), have been applied. The results indicated that employing a higher blade number and chord length enhances the starting capability of the turbine. Moreover, increasing the helical angle to 60° reduces the generated torque fluctuations. Inspired by the design of the Savonius turbine, the implementation of a J-shaped airfoil boosted the C_p at low TSR. Finally, the Kriging optimization method has been employed to optimize the design parameters explored through CFD analysis. The outcomes showed that the optimum configuration of the examined Darrieus VAWT comprises a 3-bladed rotor with a blade chord length of 0.04 m and helical angle of 0° and a J-shaped blade length ratio of 0.68. This configuration yields an 10% increase in efficiency at the optimum TSR.

Article History

Received May 3, 2023
Revised September 7, 2023
Accepted September 12, 2023
Available online November 1, 2023

Keywords:

Darrieus VAWT
Power coefficient
CFD simulation
DMST simulation
Kriging optimization

1. INTRODUCTION

Researchers have turned their attention to exploring renewable energy sources as a viable substitute for fossil fuels due to the escalating levels of greenhouse gases and the associated phenomenon of global warming. Over the past few years, renewable energy sources such as wind, solar, biomass, and geothermal energy have gained significant recognition for their prominence and potential. (Dixon & Hall, 2014). Wind power is a highly advantageous and environmentally friendly renewable energy option because of its availability in different regions therefore, there is an upward trend in harvesting power from wind energy (Abd El-Aziz, 2022; Chegini et al., 2023). In order to extract power from wind flow different kinds of wind turbines are developed. Horizontal axis wind turbines (HAWTs) operate with lift force and are the most common type (Saad & Asmuin,2014). Although HAWTs' generated power is significant, their installation and maintenance are too expensive and they are not available in urban areas (Liu et al., 2019). The disadvantages of HAWTs led to an increase in the improvement of vertical axis wind turbines (VAWTs). These particular wind turbines are not reliant on wind flow direction and their configuration and components are simpler (Hand et al., 2021). VAWTs are divided into two groups. The first category of VAWTs that rotate with drag force is Savonius VAWT which contains two or more buckets with a certain arc angle (Akhlaghi & Ghafoorian, 2022; Farajyar et al., 2023). These turbines operate with the drag force and do not need initial torque therefore, they are suitable for coupling with lift-base turbines to prepare self-starting torque (Abjadi et al., 2022; Asadi & Hassanzadeh, 2021). The second group of VAWTs works with lift forces such as Darrieus VAWT. The INVELOX wind turbines are also a type of ducted wind turbine that leverage the venturi effect to enhance wind speed at the turbine zone by up to fivefold. This increase can be accurately projected through the utilization of an

NOMENCLATURE

Symbols

V_∞	inlet flow velocity
n	number of rotations
T	torque
P	output power
R	rotor radius
H	rotor height
A	swept Area
C_p	power coefficient
c	blade chord
N	number of blades

Greek

μ	viscosity
ω	angular velocity
ρ	density
σ	solidity

Subscript

t	turbulence

Abbreviations

VAWT	Vertical Axis Wind Turbine
HAWT	Horizontal Axis Wind Turbine
CFD	Computational Fluid Dynamic
DMST	Double Multi-Stream Tube
MST	Multi-Stream Tube
TSR	Tip Speed Ratio
URANS	Unsteady Reynolds Averaged Naiver Stokes
LR	Length Ratio

appropriate deep learning model (Ramesh Kumar & Selvaraj, 2023). Efficiency enhancement of Darrieus VAWTs was crucial for researchers; therefore, the effect of changing different geometrical parameters such as blade chord length, airfoil profile, etc. have been evaluated (Du et al., 2019). An empirical study on the effect of the blade chord length of an H-rotor Darrieus VAWT proved that as the chord length increased, the power coefficient of the turbine rose in various wind velocity values (Ibrahim et al., 2020). Also, numerical results indicated that in small TSR values, the rotor with a more considerable blade chord length had better performance; however, the efficiency of the turbine with an enormous blade chord length value declined in high TSR values (Ghiasi et al., 2022). The number of blades is another important geometrical parameter and a Darrieus rotor with four blades had higher C_p values in small TSRs but, at high rotational speeds the efficiency of a four-bladed turbine decreased remarkably (Bel Mabrouk & El Hami, 2019). Generally, growth in turbine solidity, which is related to blade chord length and blade, enhances Darrieus turbine efficiency (Sagharichi et al., 2018; Asadbeigi et al., 2023). Blade airfoil is another important feature of the Darrieus turbine because the maximum thickness of different airfoils affects flow separation and also lift force (Abdulkareem et al., 2021). In another numerical simulation, NACA 0030 gives the highest C_p value at low TSRs in which thicker airfoil had superior performance at low TSRs due to the long duration of attached flow which led to rapid vortex shedding and huge tangential force (Subramanian et al., 2017). Also, J-shaped airfoil profiles which are a section of a complete airfoil profile showed better performance compared to common NACA airfoils. Also, straight-blade Darrieus turbines can be converted to helical VAWT to increase starting torque and reduce turbine vibrations (Akhlagi et al., 2022). Also, a proper turbulence model is necessary to capture flow behavior and determines the accuracy of numerical simulation. The results show that k-epsilon Realizable and k-omega SST can provide a suitable prediction of turbine behavior (Daróczy et al., 2015). Utilizing optimization methods in wind turbines for attaining a sufficient model to find the optimum configuration and operating conditions would reduce cost and time in simulations. A comparison between the response surface and the Kriging models showed that the Kriging model is more able to obtain precise predictions (Mehrpooya et al., 2023).

In the current numerical investigation, a novel dual CFD and DMST approach is nominated in order to study the influence of design and geometrical parameters including the blade number, blades chord length, helical angle, and J-shaped airfoil length ratio, which is considered as one of the state-of-the-art shapes for blade airfoil profile on the performance of Darrieus turbine. Also, an appropriate optimization method is selected to find the optimum configuration and parameters' sensitivity to the power coefficient. While the CFD and DMST techniques have been separately utilized in previous Darriues turbine studies, the dual CFD and DMST numerical modeling, which have only rarely been investigated, as well as the comparison of each method's potential for flow prediction and, ultimately, the optimization of the turbine geometry based on the well-predicting numerical model, constitute the study's primary novelties.

2. PROBLEM DESCRIPTION AND GEOMETRY

This study employs a three-dimensional numerical solution to assess the aerodynamic performance and analyze the impact of various geometrical features on a Darrieus VAWT with two different approaches, CFD and DMST. The CFD simulation is derived from discretization of the Navier-Stokes equations, and the DMST is based on the potential solution that was performed in Qblade. The Qblade is an open-source simulation software that utilizes the Double Multi-Stream tube (DMST) algorithm for VAWT simulation. The dimensions and features of the studied rotor, conducted experimentally by Danao et.al (Danao et al., 2013) are presented in Table 1.

The listed features in Table 1 were set as the base of the simulations. In addition, the moment of inertia was neglected due to the main purpose of the study and its low

Table 1 Key characteristics of the studied turbine

Features	Value
Rotor radius [mm]	350
Blade span [mm]	600
Blade chord length [mm]	40
Number of blades	3
Blade profile	NACA 0022
Solidity	0.34
Wind velocity [m/s]	7

effectiveness in higher tip speed ratios. Different parameters' effects on the proposed turbine were investigated by CFD and DMST methods and the obtained results were compared. It is noteworthy that, the rotor shaft, arms, and end plates were omitted in the numerical simulation. Also, the effect of air pressure and temperature was not considered.

3. GOVERNING EQUATIONS

3.1 CFD Turbulence Modeling and Fluid Mechanic Equations

The simulation is based on 3D incompressible flow. The Unsteady Reynolds Average Navier Stokes (URANS) equations govern the airflow in this study. Equations 1 and 2 demonstrate the continuity and conservation of momentum equations respectively (Siddiqui et al., 2015).

$$\nabla.\vec{v} = 0 \tag{1}$$

$$\nabla.(\vec{v}\vec{v}) = -\nabla p + \nabla.(\bar{\bar{\tau}}) + \rho\vec{g} \tag{2}$$

Where,

$$(\bar{\bar{\tau}}) = (\mu + \mu_t)\left[\nabla\vec{v} + (\nabla\vec{v})^T - \frac{2}{3}\nabla.\vec{v}I\right] \tag{3}$$

Where $\vec{\boldsymbol{v}}$ is the velocity, p and ρ are pressure and the fluid density, respectively. $\bar{\bar{\boldsymbol{\tau}}}$ is stress tensor, $\boldsymbol{\mu}$ is dynamic viscosity. $\boldsymbol{\mu_t}$ and $\boldsymbol{I}$ are turbulent viscosity and identity matrix, respectively.

In the CFD model, the k-ω turbulence model is widespread and frequently adapted for low Reynolds numbers. The utilization of this model occurs primarily in the vicinity of the wall region, where it effectively predicts turbulence within the boundary layer sub-layer. Considering the significance of the stall phenomenon at low Reynolds numbers, which is the operational range for VAWTs, the blade's aerodynamic behavior is more accurately predicted by employing the k-omega SST model, which combines elements of both the k-epsilon and k-omega models. The model effectively captures the characteristics observed in proximity to the airfoil wall and areas with separated flow. The SST k-ω model is explained (Nichols, 2010):

$$\frac{\partial k}{\partial t} + U_i\frac{\partial k}{\partial x_i} = \frac{\partial}{\partial x_i}\left[\left(\nu + \sigma_k\nu_t\right)\frac{\partial k}{\partial x_i}\right] + P_k - C_\mu\omega k \tag{4}$$

$$\frac{\partial \omega}{\partial t} + U_i\frac{\partial \omega}{\partial x_i} = \frac{\partial}{\partial x_i}\left[\left(\nu + \sigma_\omega\nu_t\right)\frac{\partial \omega}{\partial x_i}\right] + \gamma\frac{\omega}{k}P_k - \beta\omega^2 + (1-F_1)\frac{2\sigma_\omega}{\omega}\frac{\partial k}{\partial x_i}\frac{\partial \omega}{\partial x_i} \tag{5}$$

The transport equations coefficients are formulated as a combination of two distinct models. The blending function F_1 is:

$$F_1 = \tanh(\arg_1^4) \tag{6}$$

Where,

$$\arg_1 = \min[\max\left(\frac{\sqrt{k}}{C_\mu\omega y}, \frac{500\nu}{y^2\omega}\right), \frac{4\rho\sigma_{\omega^2}k}{CD_{k\omega}y^2}] \tag{7}$$

Here y represents the perpendicular distance from the wall. $CD_{k\omega}$ is formulated as the cross-diffusion term positive part:

$$CD_{k\omega} = \max\left(2\rho\sigma_{\omega^2}\frac{1}{\omega}\frac{\partial k}{\partial x_i}\frac{\partial \omega}{\partial x_i}, 10^{-20}\right) \tag{8}$$

The coefficients σ_k, σ_ω, β and γ represented in Eq.5 and 6 are calculated by:

$$\phi = F_1\phi_1 + (1-F_1)\phi_2 \tag{9}$$

The coefficients of ϕ_1 and ϕ_2 pertain to the k-ω and k-ε, respectively. Based on SST approach, the eddy viscosity is defined as:

$$\nu_t = \frac{a_1 k}{\max(a_1\omega, \Omega F_2)} \tag{10}$$

Here Ω, is the magnitude of the vorticity vector. The calculation of the coefficient F_2 is performed using the subsequent equation:

$$F_2 = \tanh(\arg_2^2) \tag{11}$$

Where,

$$\arg_2 = \max\left(\frac{2\sqrt{k}}{C_\mu\omega}, \frac{500\nu}{y^2\omega}\right) \tag{12}$$

The constants, C_μ and a_1, have values of 0.09 and 0.31, respectively.

3.2 DMST Model Equations

The DMST model is based on the MS (multi-stream) model in which the actuator disc divides into two parts of upstream and downstream. The DMST model diagram is represented in Fig. 1. This model assumes that velocity in actuator disks is constant and also the middle pressure is equal to asymptotic pressure. The Bernoulli equation governs the upstream disk. This model possesses some drawbacks like assuming steady flow and not characterizing the flow behavior in the whole domain. However, simplicity and low computational time are the

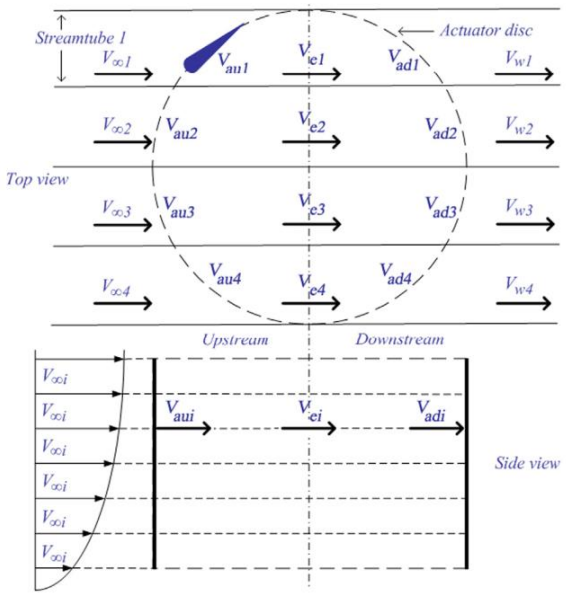

Fig. 1 DMST model diagram(Moghimi & Motawej, 2020)

advantages of this model to evaluate the vertical axis wind turbines' performance.

According to Fig. 1, the undisturbed flow stream velocity is represented by $V_{\infty i}$, which decreases in the axial direction. Also, V_{aui} is induced upstream velocity. While the flow reaches the middle of the disk it has an equilibrium velocity of V_{ei} and at downstream it becomes V_{adi}. The mentioned velocity equations are represented below (Moghimi & Motawej, 2020):

$$V_{aui} = auV_{\infty i} \tag{13}$$

$$V_{ei} = (2au-1)V_{\infty i} \tag{14}$$

$$V_{adi} = ad(2au-1)V_{\infty i} \tag{15}$$

The flow tube is modeled in the DMST approach with the interference coefficients au and ad which relate the velocities to each other.

3.3 Mathematical Equations

The tip speed ratio (TSR) which represents the ratio between wind velocity and turbine blade tip speed is defined as:

$$TSR = \frac{R \times \omega}{V_{in}} \tag{16}$$

The power coefficient (C_p), a dimensionless parameter, is defined as the ratio between the maximum output power and the passing kinetic energy flux through the front area of the turbine. Its mathematical representation is as follows:

$$C_P = \frac{P}{\frac{1}{2}\rho A V_{\infty}^3} \tag{17}$$

Where ρ (kg/m^3) density of air, V_∞ (m/s) is wind velocity, and A (m^2) represents the swept area.

The power (P) is determined by multiplying the produced torque in the turbine by the angular speed.

The solidity, an essential factor for defining rotor design and assessing turbine efficiency, is calculated using the following formula:

$$\sigma = nc / R \tag{18}$$

The variable n represents the number of blades, c donates the length of the blade chord, and R is the rotor radius.

4. NUMERICAL MODELING AND SIMULATION

4.1 DMST Modeling

For DMST analysis, the component of Qblade software is demonstrated in Fig. 2(a). The airfoil information is provided by the XFOIL direct analysis module which calculates the aerodynamic coefficients of the selected airfoil such as lift, drag, torque, and lift-to-drag coefficients. The lift and the drag coefficients are necessary to perform the simulation. The generated graph by the XFOIL module is called polar. In the next step, the blade design is accomplished by extending the selected NACA 0022 airfoil 3D blade. The blades with the dimensions given in Table 1 are divided into 20 equal sections with setting the blade number, airfoil, blade chord length, rotor radius, rotor height, twist angle, circle angle, and P-axis for each section in which for straight Darrieus the values are the same for each part. The designed blade is depicted in Fig. 3 (b).

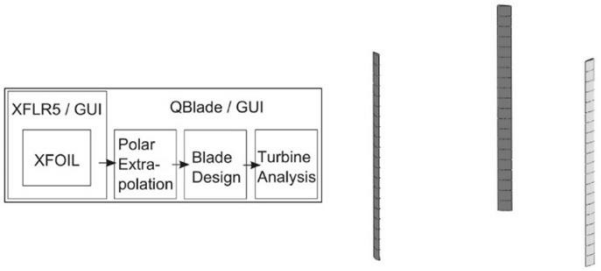

(a) (b)

Fig. 2 (a) Schematic of Qblade module, (b) Qblade blade design

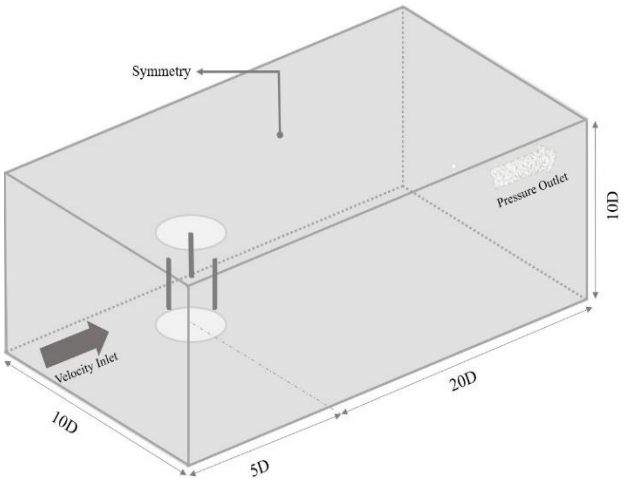

Fig. 3 Computational domain schematic

Table 2 Rotor specifications and conditions in Qblade

Features	Value
Air density (at 25°) [kg/m3]	1.225
Air viscosity [Pa.s]	1.85E-6
Max Epsilon	1E-6
Relaxation factor	0.2
Reynolds number	18000
Mach number	0.015

The rotor specifications and setup conditions other than geometrical features represented in Table 1 are represented in Table 2. Note that the more sections the blade is divided into, the more DMST simulation is done accurately. However, it imposes a higher computational cost. The polar graph generated is extended to the 360° polar extrapolation module to perform the DMST algorithm.

Afterward, the generated turbine was studied by the Multiparameter Double Multiple Streamtube (MDMS) modules to calculate the power coefficient with a wind velocity of 7 m/s in the range of TSRs with 0.025 intervals. This simulation provides 7 seconds of rotor rotation time with an average power coefficient of 0.36.

4.2 CFD Modeling

4.2.1 Boundary Condition

Due to the interaction and movement of blades and creation of the wake flow at turbine downstream, a transient simulation is adopted. The surfaces of the blades are simulated as non-slip walls. This CFD study strategically employs a constant rotational speed approach to enhance computational efficiency while avoiding the intricate challenges often associated with time-dependent simulations and variable rotational speeds. The stator inlet, positioned upstream of the rotor, is designated as the boundary condition for the velocity inlet, incorporating medium turbulence intensity. The downstream section of the stationary domain was considered as a pressure outlet with an averaged static pressure of 1 atm. The stator remains surfaces are assumed to have the symmetry condition. The rotor and stator interfaces are appropriately coupled with each other as a fluid-fluid interface with a general connection model as recommended in Ref. (Cai et al., 2019). The computational domain schematic with visual boundary conditions is depicted in Fig. 3.

Regarding Fig. 3, the cylindrical body which involved the blades is located at a proper distance from the side edges and outlet of the stator so that the wake flow downstream of the rotor can be developed. Also, the stator width and height were equal to 10D, and the length of the stator is 25D. The distance between the inlet and the center point of the rotor is 5D (Rezaeiha et al., 2017).

4.2.2 Solver Setting

The current CFD simulation conducted by ANSYS CFX v22.2, the transient scheme was chosen to reach accurate prediction. To attain a more precise solution for transient simulation, a time step of 0.0001s as 0.5° rotor rotation was determined for all simulations as suggested in Ref. (Balduzzi et al., 2016). The turbulence model was selected as SST k-ω which was discussed previously. The convergence criteria for this analysis were set to RMS with a residual of 10E-5. Also, the high-resolution advection scheme is implemented, while the second-order backward Euler scheme is utilized for the transient simulations. The simulations were run using 48 Intel Xeon 6248R 3.0 GHz cores in parallel processing.

Table 3 Comparative analysis of 3D grid properties

Reference	y^+	Airfoil mesh size	Mesh type
(Sagharichi et al., 2018)	y^+~0.83	5% chord length	Unstructured
(Tunio et al., 2020)	y^+ <1	5% chord length	Unstructured
(Dessoky et al., 2019)	y^+ <1	2.5% chord length	Structured
(Lositaño & Danao, 2019)	y^+~30	0.5% chord length	Unstructured
(Berkache et al., 2022)	y^+ ~1	1% chord length	Structured

4.2.3 Grid Independency and Validation

To effectively capture the flow behavior and crucial physical phenomena, especially around the blades the computational domain was grided with high quality. Table 3 lists a comparative analysis of various 3D grid properties obtained from previous literature. The primary objective of this comparative analysis was to ascertain whether any broad patterns or trends could be identified within the cases under consideration.

Based on the findings presented in Table 3, a clear pattern emerges where y+ values below 1 are predominantly favored in most cases. Furthermore, the airfoil mesh size is consistently observed to fall within the range of 1% to 5% of the blade chord length. However, it is important to note that the choice of mesh type displays significant variability, and a definitive basis for this diversity remains elusive.

Our grid generation was performed by ANSYS-Mechanical with affordable computational cost. An unstructured mesh with triangular elements was generated in whole domains to minimize skewness and keep this value below 0.85. The inflation layers with quadrilateral grids are generated around the airfoils wall with precise dimensions to ensure capturing the crucial sub-viscous layer and flow separation. By moving away from the airfoil, the size of the grids gradually increased with a global growth rate of 1.15. To ensure appropriate coupling between the rotational zone and the stationary zone, grids in this area are generated as non-conformal interfaces. A detailed view of grid distributions is demonstrated in Fig. 4.

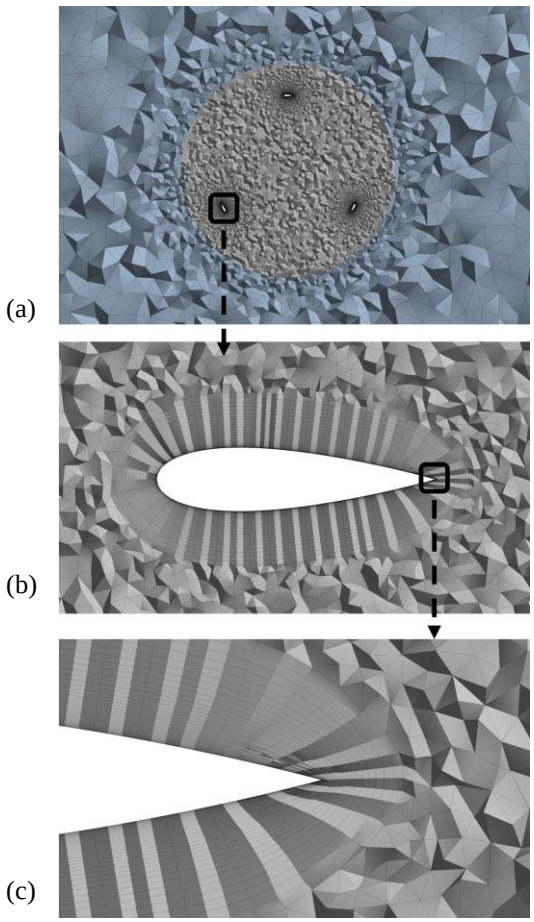

Fig. 4 2D view of generated mesh: (a) Rotating zone, (b) Around blade, (c) Trailing edge

Table 4 Mesh independency analysis

Mesh Characteristics	Mesh 1	Mesh 2	Mesh 3
Total elements number	5.1M	6.8M	8.2M
Airfoil mesh size [mm]	0.7	0.5	0.4
First layer thickness [mm]	0.015	0.010	0.007
Inflation Growth factor	1.1	1.07	1.055
Inflation layers	28	37	49
Averaged y^+	0.62	0.41	0.23
C_p	0.180	0.168	0.163

To guarantee numerical solution grid independency performed in three different cases. Since the grid quality around the airfoils has an impact on the accuracy of the results, mesh cases vary in grid density around the airfoils. Table 4 presents the specifications of the mesh configurations utilized in this study.

As seen in Table 4, to affirm mesh results accuracy, the y^+ dimensionless parameter was considered. For different turbulence models, different y^+ values are recommended. The k-ω turbulence model requires y^+ close to 1. Also, variation in power coefficient value, as well as skewness value which kept below 0.80 in different cases, were evaluated. The maximum C_p error between different

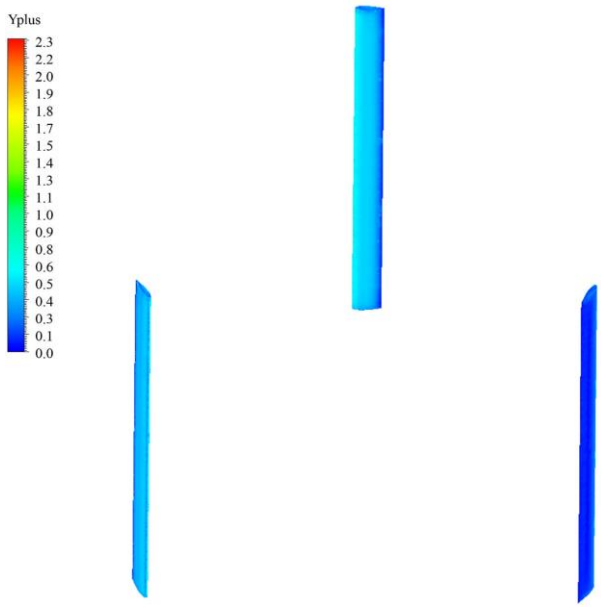

Fig. 5 Wall y+ contour around the blades

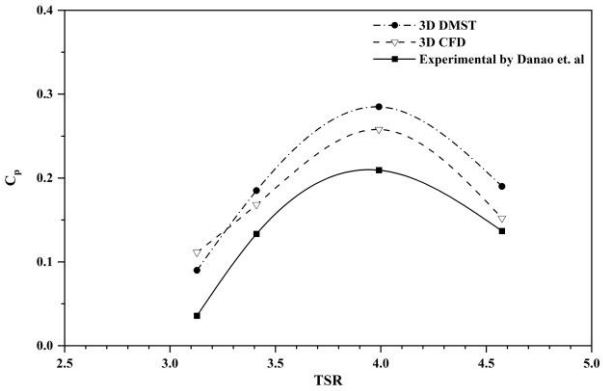

Fig. 6 C_p values from CFD and DMST simulations compared to the experimental data

meshes was 6.6% which declares a reliable mesh independence test. Therefore, Mesh 2 case was selected for the following simulation in order to attain accurate results with affordable computational time. Also, Fig. 5 depicts the y^+ distribution around the blades with the selection of the Mesh 2 case.

As demonstrated in Fig. 5, the maximum y^+ value is around 2.3 and some parts of the leading edge and trailing edges have y^+ below 1.

The experimental measurements of Darrieus VAWT studied by Danao et al (Danao et al., 2013) were nominated for validating current numerical simulation. The characteristics of the Darrieus rotor for CFD investigation was represented in Table 1. For the validation, Mesh 2 case was selected with a time step of 0.0001s corresponding to 0.5° rotor rotation. Figure 6 showcases the comparative analysis of numerical CFD, DMST, and experimental findings across four distinct TSRs.

It can be concluded from Fig. 6 that the results of the CFD and DMST show a satisfactory agreement with

experimental study data. However, the DMST model overestimates the power coefficient compared to experimental data. The CFD and DMST methods captured the experimental curve and both reach maximum C_p at λ=4. The overprediction of the C_p in the 3D CFD model is due to the RANS model weakness, especially in low TSRs where dynamic stall occurs. The DMST model's overestimation of the power coefficient results from the model's simplicity, as was addressed in section 3.2, although this method accurately predicted the flow behavior. Hence, the validity of the CFD and DMST analysis can be confirmed.

5. RESULTS AND DISCUSSION

In this section of the study, the investigation focused on analyzing the impact of geometrical parameters on the aerodynamic performance of the VAWT under investigation. These parameters are the blade number, blade chord length, helical angle, and J-shaped airfoil. This numerical study has been done with the help of CFD and DMST numerical methods.

5.1 Effect of Blade Number

The rotor blade number is a critical design factor which exerts a substantial influence on the aerodynamic performance of wind turbines, which has a direct effect on the system's solidity. Figure 7 shows the effect of the blade number on system performance.

Regarding Fig. 7 number of blades significantly affects Darrieus VAWT aerodynamic performance and C_p values.

The findings demonstrated that the rotor configuration featuring a greater number of blades at the initial TSRs performed significantly better. However, when the rotational velocity increased, this trend was reversed and the rotor with a lower number of blades which has less solidity showed more productivity. At λ=3.1, the C_p value of the five-bladed turbine has experienced a 29% rise compared to the standard three-bladed turbine, while at TSR=4.6, this configuration has experienced a 13% decrease in C_p value compared to the standard geometry. The high values of the power coefficient in the initial TSRs can indicate that the rotor initial torque is higher which can solve the turbine's self-starting inability. Figure 8 showcases the results obtained from the DMST

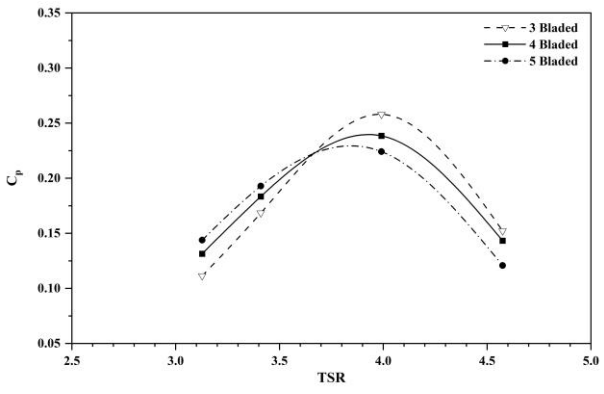

Fig. 7 Effect of blade number on power coefficient

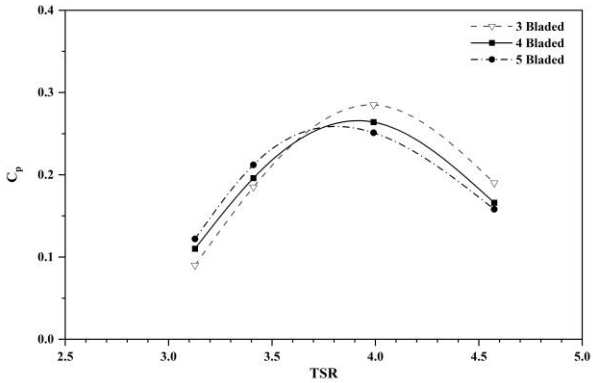

Fig. 8 Effect of blade number on power coefficient with DMST approach

numerical solution, illustrating the impact of varying blade numbers on the turbine performance.

As it is clear from the results, the trend of changes in C_p values with the DMST solution method is similar to the results obtained from the CFD solution. This indicates that, in the initial TSRs, the turbine with a higher solidity outperformed other configurations. However, with the increase in TSR values, this trend is reversed. Based on this figure at λ=3.1, the C_p value related to the rotor with five blades is 33% more than standard geometry. The noticeable point is that the DMST solution overpredicts the power coefficient. The root of the difference in CFD and DMST results is the inability of the DMST solution to simulate wake flow around and at downstream of the rotor while increasing the solidity which intensely increases the wake. As this numerical method is based potential solution, the model lacks the capability to accurately simulate the flow pattern in the wake region downstream of the rotor and since the wake flow reduces the efficiency, failure to consider this phenomenon has caused errors in the results. For a better understanding of the effect of adding blades to the rotor and to clarify the importance of wake flow, the velocity contour plot for each geometry at λ=4, which is the state of maximum power obtained from each turbine, is shown in Fig. 9.

Regarding Fig. 9, the intensity of the wake flow, which is known as a low-speed region, is quite noticeable in the space between the blades in the configuration with five blades. This low-speed area reduces the efficiency of the system. Also, the wake flow in the rotor downstream of the five-bladed rotor is strongly concentrated. Furthermore, in turbines with a higher solidity, the wake

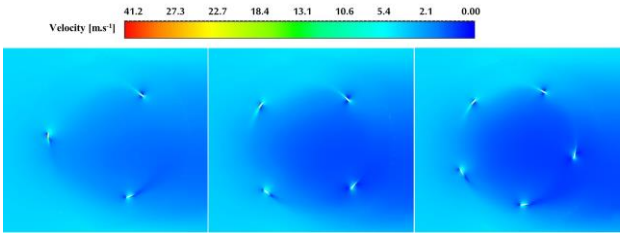

(a) (b) (c)

Fig. 9 Velocity contour for different configurations at λ = 4: (a) 3-bladed, (b) 4-bladed, (c) 5-bladed

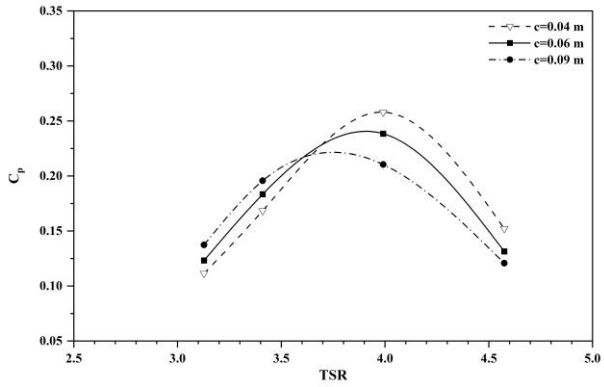

Fig. 10 Effect of blade chord length on power coefficient

flow at the behind each blade at the trailing edge has an impact on the front section of the rear blade at its leading edge, this phenomenon called blade-to-blade interaction causes a decrease in turbine efficiency, especially at high angular velocities.

5.2 Effect of Blade Chord Length

This section of the study delved into the examination of blade chord length effect on aerodynamic performance and Darrieus VAWT efficiency was investigated by studying three different blade chord lengths of 0.09 (m), 0.06 (m), and 0.04 (m). The results of the effect of blade chord length on system efficiency are given in Fig. 10.

Looking at the information in Fig. 10, the utilization of larger chord lengths, resulting in an increase in blade Reynolds number, has been observed to correspond to higher C_p values at low TSRs. The trend of C_p changes is similar to the variations in the number of blades. One additional consequence of increasing the solidity of rotor is that a greater blade surface interacts the airflow, leading to increased energy generation. At the starting point of the turbine λ=3.1, the C_p value of the rotor with a 0.09 (m) chord length raised 23% compared to the standard rotor, whereas at λ=4.6, this configuration has experienced a 18% decline in C_p value compared to the standard geometry. The DMST solution model also was used to explore the influence of blade chord length on Darrieus' performance, and the results are shown in Fig. 11.

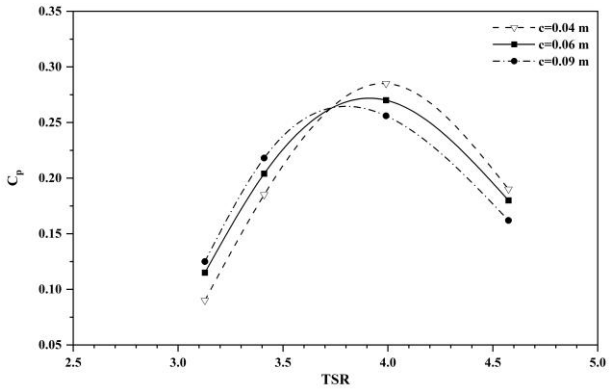

Fig. 11 Effect of blade chord length on power coefficient with DMST approach

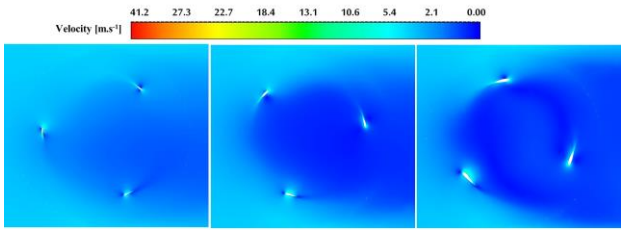

(a) (b) (c)

Fig. 12 Velocity contour for different configurations at λ = 4: (a) c=0.04 (m), (b) c=0.06 (m), (c) c=0.09 (m)

As for the data in Fig. 11, the C_p trend as a function of TSR with blade chord length variations follows the trend of CFD results. It means in the initial TSR higher solidity turbine with a higher blade chord length value exhibits superior performance compared to other configurations. It is also stated from the results that at λ=3.1, the C_p value of the turbine with a blade chord length of 0.09 (m) is 37% higher than the C_p of the turbine with a blade chord length of 0.04(m). It should be emphasized again that the results of the DMST solution give higher values for C_p in the same TSR and the reason for this problem is not considering the wake flow downstream of the turbine and blades, which is a fundamental weakness for this potential solution. To demonstrate the impact of wake flow between the blades' space and in the downstream section of the rotor, velocity contour plots are given for different rotor configurations with various blade chord lengths based on the CFD method at TSR=4 in Fig. 12.

Figure 12 shows the velocity contour around blades at λ=4. In the condition where the blade chord length is increased, not only the phenomenon of the blade-to-blade interaction is augmented and the wake flow produced at the trailing edge of upstream blade affect the trailing edge of the downstream blades, but also the low-speed zone between the blades increases significantly. It has been found that this reduces the efficiency of the turbine at high rotational velocity. Also, by growing blade chord length value, the wake flow at the downstream section of the turbine intensifies further. which remarkably declines system productivity.

5.3 Effect of Helical Angle

In this section, a comprehensive investigation is conducted to analyze the influence of the helical angle on the aerodynamic performance and overall efficiency of the Darrieus rotor. Note that standard Darrieus twisted with a certain helical angle while keeping the other parameters constant. Therefore, helical angle values of 30° and 60° are examined to discover the turbine behavior. It should be mentioned that the DMST model conducted by Qblade was unable to capture variation in power coefficient for different helical angles. The power coefficient results of different helical angles are given in Fig. 13.

From the data in Fig. 13, applying the helical angle on the turbine blades in the early TSRs increases the efficiency compared to the straight blade turbine in which at starting point λ=3.1 the C_p value corresponding to the turbine with 60° helical angle is 13% higher than the turbine with straight blades which states higher initial

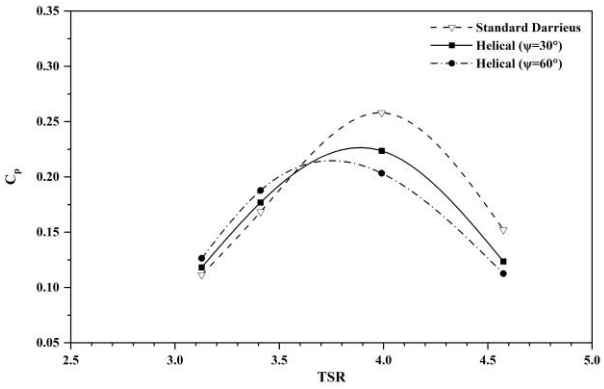

Fig. 13 Effect of helical angle on power coefficient

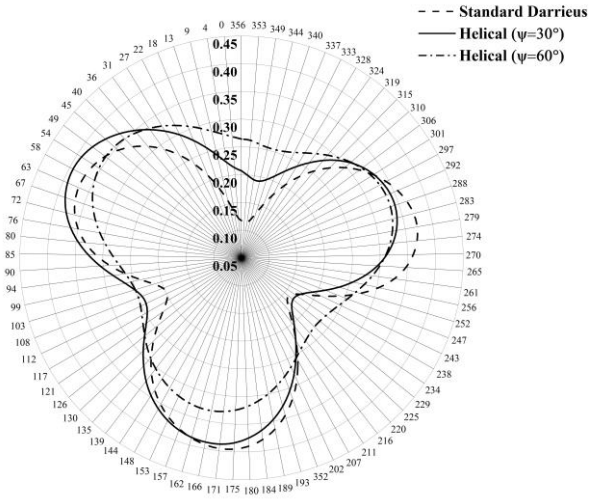

Fig. 14 Torque of different helical angles at λ = 3.1

torque for turbine starting. However, as the angular velocity increases, this trend is reversed and straight blade Darrieus attained better performance in which at λ=4.6, obtained C_p for rotor with 60° helical angle blade is 21% less than straight blade rotor. To illuminate the functional difference between a straight Darrieus and a helical turbine, the three-blade torque value in one rotation at initial TSR is plotted in Fig. 14.

It can be concluded from Fig. 14 that, by increasing the helical angle to 60°, a smoother torque is introduced to the shaft by the blades. This is because the straight-blade turbine exposes to the optimal position cyclically regarding the upstream flow while the helical turbine subjects a particular section of the blade to the optimal position. To illustrate the 3D effect of helical angle, the tip vortex contour of the straight Darrieus and optimal helical turbine with a 60° twist angle at initial TSR are shown in Fig. 15.

As shown in the tip vortex contour, the straight blade tip vortices are intense within the rotor. On the contrary, the helical turbine has brought smoother behavior. This phenomenon leads to a higher starting torque of the helical turbine while as rotational speed increases, the higher generated power by the straight turbine prevails over the negative effects of the tip vortex.

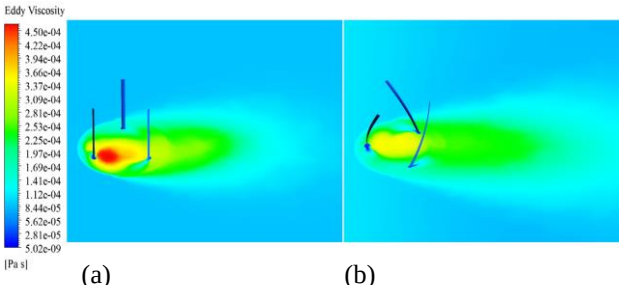

Fig. 15 Tip vortex contour at λ=3.1: (a) Standard Darrieus, (b) Helical turbine (ψ=60°)

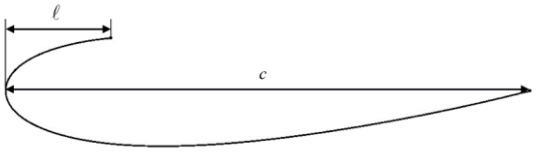

Fig. 16 J-shaped profile structure

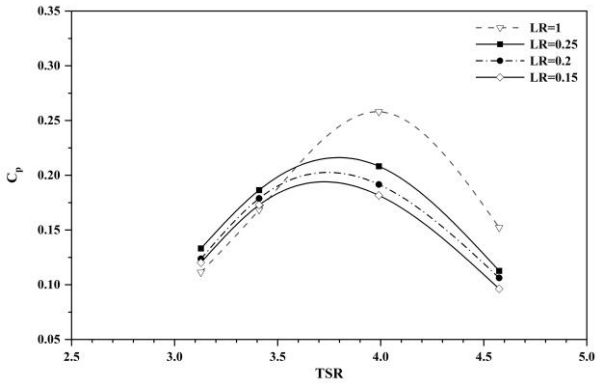

Fig. 17 Effect of J-shaped blade on power coefficient

5.4 Effect of J-shaped Blade

In this section, the study on the performance of a J-shaped profile with three different length ratios of 0.15, 0.2 and 0.25 is performed and the result is compared to the standard Darrieus. These values were obtained based on the study outlined in Ref. (Pan et al., 2021). The length ratio (LR) is the ratio between the distance from the leading edge to the end of the upper surface and the chord length. The schematic of the J-shaped airfoil structure is demonstrated in Fig. 16.

The J-shaped blade utilizes lift and drag forces simultaneously at certain azimuth angles. The power coefficient results for the variation of length ratios are shown in Fig. 17. Note that LR=1 corresponds to the standard Darrieus turbine.

From Fig. 17 it observed that by using J-shaped blades the starting torque of the turbine improved significantly and a 19% improvement in power coefficient was obtained by optimum J-shape airfoil compared to standard Darrieus. From λ=3.6 the augmentation in the power coefficient decreases and by increasing TSR, the standard Darrieus will attain the maximum poswer coefficient.

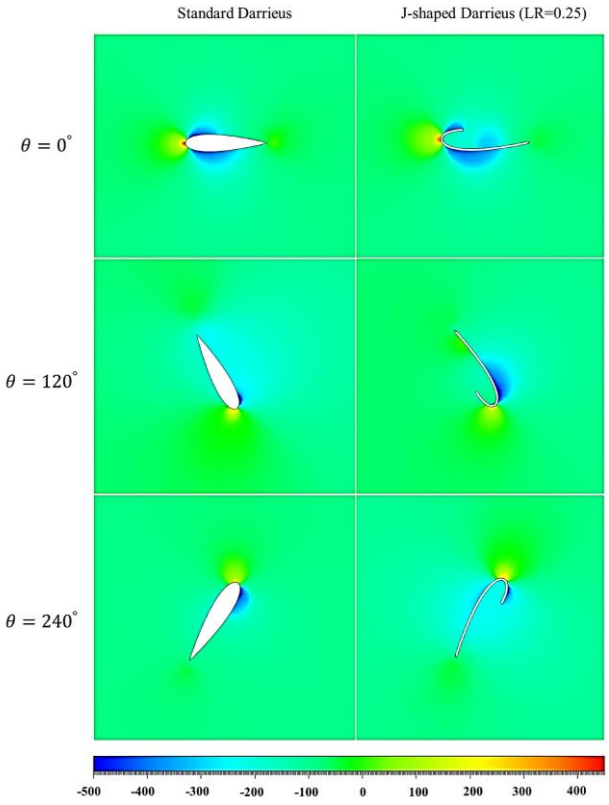

Fig. 18 Pressure contour at λ=4 for standard Darrieus and J-shaped profile with (LR=0.25) in different azimuth angles

Furthermore, by comparing different J-shaped profiles, it can be concluded that as the upper surface length increases, the generated power increases. However, the impact of upper surface length in low TSRs is insignificant and as the rotational speed increased the J-shaped profile with a 0.25 length ratio is tend to be like standard Darrieus which gained higher generated power. For better illustration, the pressure contour of the standard Darrieus and optimum J-shaped profile is depicted in Fig. 18.

As can be seen in Fig. 18, at θ=120 the pressure differential on the upper and the lower surface of the J-shaped profile is more significant than standard Darrieus which generated higher torque. In addition, a J-shaped profile eliminates the pressure side of the upper surface and improves lift force generation. The pressure difference between the leading and trailing edges increased which led to generating drag force and boosting torque generation and enhancing the turbine's capability for self-starting. At the θ=240, the J-shaped profile decreased the negative pressure at the upper surface and increased it at the lower surface compared to the standard Darrieus and enhanced torque value.

6. OPTIMIZATION

In this section, the proposed Darrieus with 4 studied parameters is selected to find the optimal geometric characteristic to achieve maximum efficiency. Noted that the CFD studied parameter was chosen for optimization due to higher precise results. Various optimization methods were recommended to suggest optimum conditions based on the design of experiments. Among the optimization methods, response surface model (RSM), Genetic aggregation, and Kriging method are chosen to compare the capability of the models which is determined by fitting error. The RSM benefits second-order polynomials as an approach for approximation, Genetic aggregation is based on computing response surface and Kriging is introduced as a viable alternative, offering a statistical approximation method. These three mentioned models were analyzed to make a comparison between the accuracy of the results. Based on the previous CFD results, a total of 40 design points have been carefully considered for the purpose of executing optimization models, thus serving as crucial input variables. These points are derived from observed simulated points which constitute variables of tip speed ratio, blade number, blade chord length, helical angle and J-shaped length ratio. Table 5 shows the error analysis of three analyzed models.

Table 5 Analysis of errors

Model	Coefficient of Determination	Root MSE
2nd order RS	0.9381	0.01061
Genetic Aggregation	0.9992	1.145E-04
Kriging model	1	3.133E-09

The analysis of Table 5 leads to the conclusion that the Kriging method exhibits a lower Root Mean Square Error (RMSE) with a higher coefficient of determination compared with other models. Hence, the Kriging method provides the most accurate estimation of values at unobserved locations. Therefore, the Kriging optimization model is nominated to discover the optimum Darriues parameters and to evaluate responses. According to the main focus of the study, the objective function of the optimization model is defined as maximizing the turbine's power coefficient. Figure 19 depicts the graphical response C_p curves obtained from the Kriging model, for the various points.

Figure 19 vividly illustrates the dynamic relationship between the response variables and the changing input variables. Furthermore, the power coefficient local sensitivity to the input variables was attained. This is performed by varying one input variable at a time while keeping the others constant. The pie chart result is represented in Fig. 20.

As evident in Fig. 20, the J-shaped length ratio exhibited the highest sensitivity of power coefficient which was particularly demonstrated at high rotational speeds. The helical angle followed as the second parameter in terms of sensitivity to the power coefficient with the value around 10%. Furthermore, it is deduced that the blade number factor exerts the least significant influence on the C_p. It should be noted that the structural considerations and rotor weight were not taken

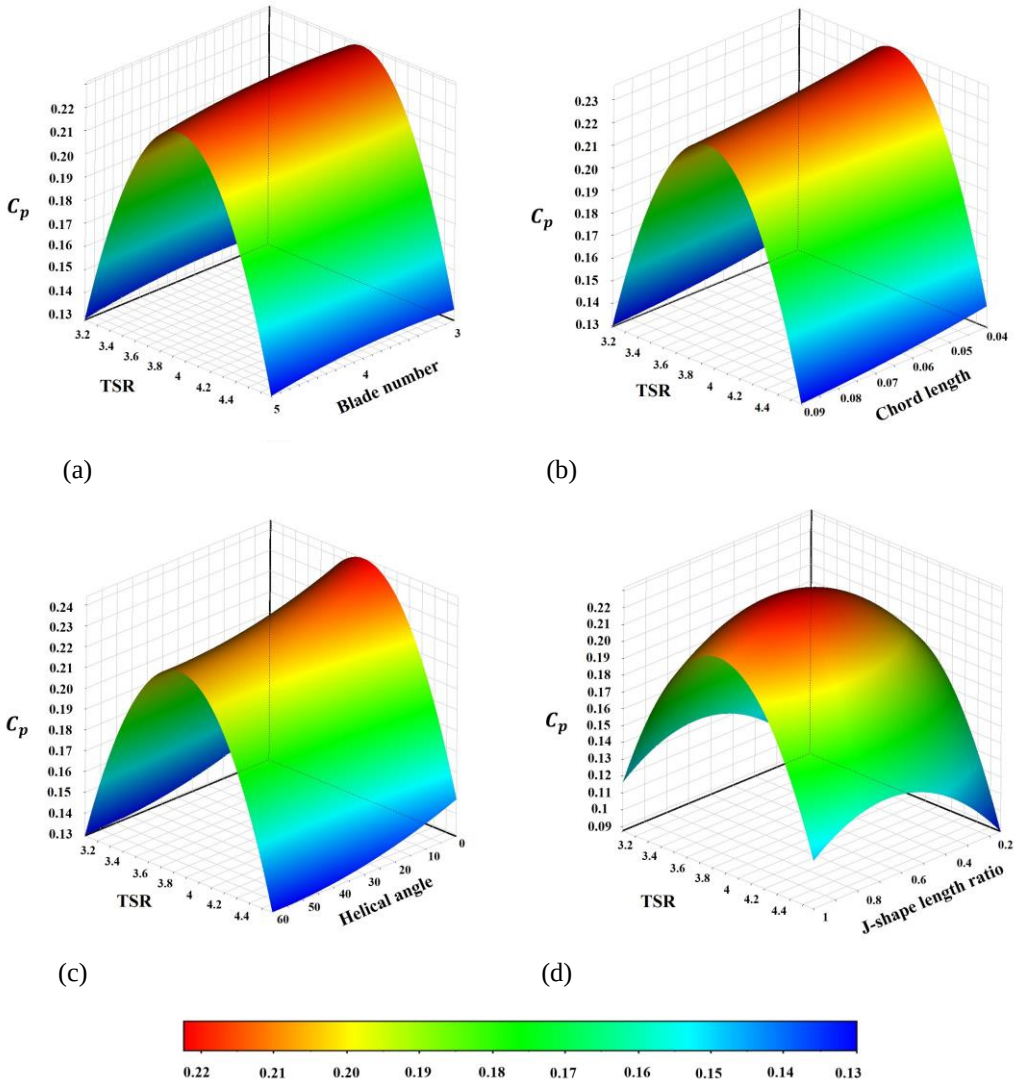

Fig. 19 Power coefficient variation with TSR (a) Blade number (b) Chord length (c) Helical angle (d) J-shaped length ratio

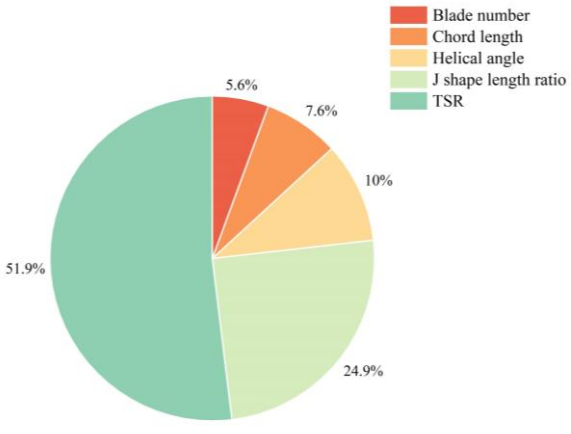

Fig. 20 Local sensitivity

into account. Finally, the optimum geometric features suggested by the Kriging method has provided in Table 6.

It has shown that at around λ=4 the maximum power with mentioned features can be generated with the rotor. The predicted C_p value for the optimum rotor was reported around 0.285 which improved efficiency at optimum TSR by 10%.

Table 6 Optimum geometrical and operational features derived from Kriging method

Input variables	Optimal feature
Blade number	3
Chord length [m]	0.04
Helical angle [°]	0
J shape length ratio	0.68
TSR	3.9

7. CONCLUSION

This numerical study had the primary objective of conducting a parametric investigation and optimization of the Darrieus wind turbine to enhance its performance. To accomplish this objective, the impact of four key geometrical parameters, which include the number of blades, blade chord length, helical angle, and the J-shaped blade length ratio, was thoroughly examined with regard to their influence on the aerodynamic performance of the proposed Darrieus VAWT. This investigation was conducted using dual CFD and DMST models, allowing for a comprehensive analysis and comparison of accuracy

and output results. The outcomes of this study are concisely summarized below.

- The utilization of a higher number of blades enhances its solidity, leading to improved performance in the initial TSRs and improving its self-starting ability. A 5-bladed turbine was able to achieve a notable 29% increase in power in initial TSR. However, the 3-bladed turbine demonstrated maximum C_p at optimal TSR.
- The higher blade chord length in the initial TSRs augmented the torque generation which turbine with c= 0.09 m augmented efficiency by 23%. At higher rotational speeds, a lower chord length of 0.04 m was found to achieve the optimum power coefficient.
- The turbine with 30° and 60° helical angles at early TSRs exhibit performance improvement compared to the straight-blade turbine. Helical blade turbine with $\psi=60^{\circ}$ attained 13% higher generated power compared to $\psi=0^{\circ}$. This improvement stems from the helical turbine's ability to minimize the generation of tip vortices, leading to enhanced power output.
- The implementation of the J-shape airfoil design improved the self-starting of the convectional Darrieus turbine. Increasing length ratio (LR) of J-shape profile, augmented C_p at all TSRs. J- shaped airfoil turbine with LR=0.25 boosted starting torque by 19% compared with standard Darrieus turbine.

CONFLICT OF INTEREST

The authors declare that they have no known competing financial interests or personal relationships that could have appeared to influence the work reported in this paper.

AUTHORS CONTRIBUTION

Mohammad Akhlaghi: Conceptualization, Methodology, Writing original draft, Supervision, Resources, Project administration, Funding acquisition. **Mohammadreza Asadbeigi**: Conceptualization, Methodology, Software, Validation, Data Curation, Visualization, Formal analysis, Investigation, Writing original draft, Writing review & editing. **Farzad Ghafoorian**: Conceptualization, Methodology, Software, Writing original draft.

REFERENCES

Abd El-Aziz, R. M. (2022). Renewable power source energy consumption by hybrid machine learning model. *Alexandria Engineering Journal*, *61*(12), 9447–9455. https://doi.org/10.1016/j.aej.2022.03.019

Abdulkareem, O. A., Khudheyer, A. F., & Abbas, A. S. (2021). Numerical *Investigation of the effect of changing the thickness of airfoils used in wind turbines on the lift to drag ratio*. IOP Conference Series: Materials Science and Engineering, *1094*(1), 012078. https://doi.org/10.1088/1757-899X/1094/1/012078

Abjadi, A., Ghafoorian, F., & Chegini, S. (2022). Effect of nozzle installation on the aerodynamic performance of a savonius vertical axis wind turbine, using CFD method. *Journal of Mechanical Research and Application*, *11*(4), 87–70.

Akhlaghi, M., & Ghafoorian, F. (2022). The investigation of arc angle rotor blade variations effect of the Savonius vertical axis wind turbine on the Power and Torque coefficients, using 3D modeling. *Renewable Energy Research and Applications*. https://doi.org/10.22044/rera.2022.11282.1084

Akhlagi, M., Ghafoorian, F., Mehrpooya, M., & Sharifi Rizi, M. (2022). *Effective parameters optimization of a small scale gorlov wind turbine, using cfd method*. In Iranian Journal of Chemistry and Chemical Engineering. Iranian Institute of Research and Development in Chemical Industries (IRDCI)-ACECR. https://doi.org/10.30492/IJCCE.2022.561960.5584

Asadbeigi, M., Ghafoorian, F., Mehrpooya, M., Chegini, S., & Jarrahian, A. (2023). A 3D study of the darrieus wind turbine with auxiliary blades and economic analysis based on an optimal design from a parametric investigation. *Sustainability*, *15*(5), 4684. https://doi.org/10.3390/su15054684

Asadi, M., & Hassanzadeh, R. (2021). Effects of internal rotor parameters on the performance of a two bladed Darrieus-two bladed Savonius hybrid wind turbine. *Energy Conversion and Management*, *238*, 114109. https://doi.org/10.1016/j.enconman.2021.114109

Balduzzi, F., Bianchini, A., Ferrara, G., & Ferrari, L. (2016). Dimensionless numbers for the assessment of mesh and timestep requirements in CFD simulations of Darrieus wind turbines. *Energy*, *97*, 246–261. https://doi.org/10.1016/j.energy.2015.12.111

Bel Mabrouk, I., & El Hami, A. (2019). Effect of number of blades on the dynamic behavior of a Darrieus turbine geared transmission system. *Mechanical Systems and Signal Processing*, *121*, 562–578. https://doi.org/10.1016/j.ymssp.2018.11.048

Berkache, A., Boumehani, A., Noura, B., & Kerfah, R. (2022). Numerical investigation of 3D unsteady flow around a rotor of vertical axis wind turbine darrieus type H. *Journal of Thermal Engineering*, *8*(6), 691–701. https://doi.org/10.18186/thermal.1193932

Cai, X., Zhang, Y., Ding, W., & Bian, S. (2019). The aerodynamic performance of H-type darrieus VAWT rotor with and without winglets: CFD simulations. *Energy Sources, Part A: Recovery, Utilization, and Environmental Effects*, 1–12. https://doi.org/10.1080/15567036.2019.1691286

Chegini, S., Ghafoorian, F., Moghimi, M., & Mehrpooya, M. (2023). *Optimized arrangement of clustered Savonius VAWTs, Techno-Economic evaluation and*

feasibility of installation. In Iranian Journal of Chemistry and Chemical Engineering. Iranian Institute of Research and Development in Chemical Industries (IRDCI)-ACECR. https://doi.org/10.30492/IJCCE.2023.2004246.6066

Danao, L. A., Eboibi, O., & Howell, R. (2013). An experimental investigation into the influence of unsteady wind on the performance of a vertical axis wind turbine. *Applied Energy*, *107*, 403–411. https://doi.org/10.1016/j.apenergy.2013.02.012

Daróczy, L., Janiga, G., Petrasch, K., Webner, M., & Thévenin, D. (2015). Comparative analysis of turbulence models for the aerodynamic simulation of H-Darrieus rotors. *Energy*, *90*, 680–690. https://doi.org/10.1016/j.energy.2015.07.102

Dessoky, A., Bangga, G., Lutz, T., & Krämer, E. (2019). Aerodynamic and aeroacoustic performance assessment of H-rotor darrieus VAWT equipped with wind-lens technology. *Energy*, *175*, 76–97. https://doi.org/10.1016/j.energy.2019.03.066

Dixon, S. L., & Hall, C. A. (2014). *Fluid mechanics and thermodynamics of turbomachinery* (Seventh edition). Butterworth-Heinemann is an imprint of Elsevier.

Du, L., Ingram, G., & Dominy, R. G. (2019). A review of H-Darrieus wind turbine aerodynamic research. *Proceedings of the Institution of Mechanical Engineers, Part C: Journal of Mechanical Engineering Science*, *233*(23–24), 7590–7616. https://doi.org/10.1177/0954406219885962

Farajyar, S., Ghafoorian, F., Mehrpooya, M., & Asadbeigi, M. (2023). CFD investigation and optimization on the aerodynamic performance of a savonius vertical axis wind turbine and its installation in a hybrid power supply system: a case study in iran. *Sustainability*, *15*(6), 5318. https://doi.org/10.3390/su15065318

Ghiasi, P., Najafi, G., Ghobadian, B., Jafari, A., & Mazlan, M. (2022). Analytical study of the impact of solidity, chord length, number of blades, aspect ratio and airfoil type on h-rotor darrieus wind turbine performance at low reynolds number. *Sustainability*, *14*(5), 2623. https://doi.org/10.3390/su14052623

Hand, B., Kelly, G., & Cashman, A. (2021). Aerodynamic design and performance parameters of a lift-type vertical axis wind turbine: A comprehensive review. *Renewable and Sustainable Energy Reviews*, *139*, 110699. https://doi.org/10.1016/j.rser.2020.110699

Ibrahim, K. A., El-Askary, W. A., Ghonim, T. A., & Nebiewa, A. M. (2020). An experimental investigation of a darrieus straight-bladed wind turbine. *ERJ. Engineering Research Journal*, *43*(1), 1–9. https://doi.org/10.21608/erjm.2020.72098

Liu, J., Lin, H., & Zhang, J. (2019). Review on the technical perspectives and commercial viability of vertical axis wind turbines. *Ocean Engineering*, *182*, 608–626. https://doi.org/10.1016/j.oceaneng.2019.04.086

Lositaño, I. C. M., & Danao, L. A. M. (2019). Steady wind performance of a 5 kW three-bladed H-rotor Darrieus Vertical Axis Wind Turbine (VAWT) with cambered tubercle leading edge (TLE) blades. *Energy*, *175*, 278–291. https://doi.org/10.1016/j.energy.2019.03.033

Mehrpooya, M., Asadbeigi, M., Ghafoorian, F., & Farajyar, S. (2023). *Investigation and optimization on effective parameters of a h-rotor darrieus wind turbine, using CFD method*. In Iranian Journal of Chemistry and Chemical Engineering. Iranian Institute of Research and Development in Chemical Industries (IRDCI)-ACECR. https://doi.org/10.30492/IJCCE.2023.562396.5610

Moghimi, M., & Motawej, H. (2020). Developed DMST model for performance analysis and parametric evaluation of Gorlov vertical axis wind turbines. *Sustainable Energy Technologies and Assessments*, *37*, 100616. https://doi.org/10.1016/j.seta.2019.100616

Nichols, R. H. (2010). Turbulence models and their application to complex flows. *University of Alabama at Birmingham, Revision*, *4*, 89.

Pan, L., Zhu, Z., Xiao, H., & Wang, L. (2021). Numerical analysis and parameter optimization of j-shaped blade on offshore vertical axis wind turbine. *Energies*, *14*(19), 6426. https://doi.org/10.3390/en14196426

Ramesh Kumar, K., & Selvaraj, M. (2023). Novel deep learning model for predicting wind velocity and power estimation in advanced INVELOX wind turbines. *Journal of Applied Fluid Mechanics*, *16*(6), 1256–1268. https://www.jafmonline.net/article_2221_759402dff652b08d4823872a0d974408.pdf

Rezaeiha, A., Kalkman, I., & Blocken, B. (2017). CFD simulation of a vertical axis wind turbine operating at a moderate tip speed ratio: Guidelines for minimum domain size and azimuthal increment. *Renewable Energy*, *107*, 373–385. https://doi.org/10.1016/j.renene.2017.02.006

Saad, M. M. M., & Asmuin, N. (2014). Comparison of horizontal axis wind turbines and vertical axis wind turbines. IOSR Journal of Engineering (IOSRJEN), 4(08), 2730. https://doi.org/10.9790/3021-04822730

Sagharichi, A., Zamani, M., & Ghasemi, A. (2018). Effect of solidity on the performance of variable-pitch vertical axis wind turbine. *Energy*, *161*, 753–775. https://doi.org/10.1016/j.energy.2018.07.160

Siddiqui, M. S., Rasheed, A., Kvamsdal, T., & Tabib, M. (2015). Effect of Turbulence Intensity on the Performance of an Offshore Vertical Axis Wind Turbine. *Energy Procedia*, *80*, 312320. https://doi.org/10.1016/j.egypro.2015.11.435

Subramanian, A., Yogesh, S. A., Sivanandan, H., Giri, A., Vasudevan, M., Mugundhan, V., & Velamati, R. K. (2017). Effect of airfoil and solidity on performance of small scale vertical axis wind turbine using three dimensional CFD model. *Energy*, *133*, 179–190. https://doi.org/10.1016/j.energy.2017.05.118

Tunio, I. A., Shah, M. A., Hussain, T., Harijan, K., Mirjat, N. H., & Memon, A. H. (2020). Investigation of duct augmented system effect on the overall performance of straight blade Darrieus hydrokinetic turbine. *Renewable Energy*, *153*, 143–154. https://doi.org/10.1016/j.renene.2020.02.012